Exp Fluids (2007) 43:39–51
DOI 10.1007/s00348-007-0319-x

RESEARCH ARTICLE

Spatial resolution of PIV for the measurement of turbulence

P. Lavoie · G. Avallone · F. De Gregorio · G. P. Romano · R. A. Antonia

Received: 25 September 2006 / Revised: 20 April 2007 / Accepted: 20 April 2007 / Published online: 30 May 2007

Abstract Recent technological advancements have made the use of particle image velocimetry (PIV) more widespread for studying turbulent flows over a wide range of scales. Although PIV does not threaten to make obsolete more mature techniques, such as hot-wire anemometry (HWA), it is justifiably becoming an increasingly important tool for turbulence research. This paper assesses the ability of PIV to resolve all relevant scales in a classical turbulent flow, namely grid turbulence, via a comparison with theoretical predictions as well as HWA measurements. Particular attention is given to the statistical convergence of mean turbulent quantities and the spatial resolution of PIV. An analytical method is developed to quantify and correct for the effect of the finite spatial resolution of PIV measurements. While the present uncorrected PIV results largely underestimate the mean turbulent kinetic energy and energy dissipation rate, the corrected measurements agree to a close approximation with the HWA data. The transport equation for the second-order structure function in grid turbulence is used to establish the range of scales affected by the limited resolution. The results show that PIV, due to the geometry of its sensing domain, must meet slightly more stringent requirements in terms of resolution, compared with HWA, in order to provide reliable measurements in turbulence.

P. Lavoie (✉)
Department of Aeronautics, Imperial College London, London, UK
e-mail: p.lavoie@imperial.ac.uk

G. Avallone · G. P. Romano
Department of Mechanics and Aeronautics, University ''La Sapienza'', Rome, Italy

F. De Gregorio
CIRA, Italian Aerospace Center, Capua, Italy

R. A. Antonia
Discipline of Mechanical Engineering, University of Newcastle, Callagan, NSW, Australia

1 Introduction

Non-intrusive laser-based techniques, such as laser Doppler velocimetry (LDV) and particle image velocimetry (PIV), are being used more widely for turbulence measurements. Although these techniques offer various advantages over more traditional methods (e.g. hot-wire anemometry—HWA), their ability to resolve adequately all scales of interest for turbulence studies has yet to be established rigorously, particularly in the case of PIV. It is therefore important that these techniques are properly validated, in order to assess their spatial resolution limitations and investigate the impact of advancements related to each technique. This type of approach has been successfully implemented in the improvement of LDV data reduction schemes, as they pertain to improved frequency resolution (Müller et al. 1998; Van Maanen et al. 1999). In the case of PIV, Westerweel et al. (1997) improved the spatial resolution by nearly a factor of 10, through the use of a window offset. Only very recently have there been attempts to quantify the effect of the limited spatial resolution associated with the finite size of the interrogation window in PIV (Scarano 2003; Foucaut et al. 2004; Saikrishnan et al. 2006; Poelma et al. 2006). Although PIV has demonstrated strong improvements in the description of small scales, there is still an open question relative to the

effect of resolution on its ability to capture accurately the inertial and dissipative ranges.

There are two main issues that emerge when implementing validation procedures for a particular measurement technique. Firstly, it is important to select a flow

for which theoretical results, especially in connection with the flow properties of interest (in this case, the small scales of turbulence), are known with a high level of confidence. Secondly, it is desirable to compare the technique against a method that has good temporal and spatial resolutions. With regard to the first issue, homogeneous isotropic turbulence (HIT) is ideal from a theoretical viewpoint, while a close approximation of this flow is provided by the decaying turbulence downstream of a grid. Much has been learned from the previous works on grid turbulence since the seminal papers by Batchelor and Townsend (1947, 1948), and Comte-Bellot and Corrsin (1966). However, some aspects of this flow remain unclear, such as the possible dependence of the turbulence statistics on initial conditions (e.g. the shape and size of the grid mesh, see for instance the thorough discussions given by George et al. 2001). Notwithstanding these possible effects, the turbulent kinetic energy dissipation rate (simply dissipation hereafter) can be estimated indirectly with high accuracy from the kinetic energy budget (Corrsin 1963),

$$\langle \varepsilon \rangle_d = -\frac{U}{2}\frac{\mathrm{d}\langle q^2 \rangle}{\mathrm{d}x_1}, \tag{1}$$

where U is the mean flow velocity, $\langle q^2 \rangle (\equiv \langle u_1^2 \rangle + \langle u_2^2 \rangle + \langle u_3^2 \rangle)$ is twice the turbulent kinetic energy, $\langle\rangle$ denotes time averaging and the subscript d indicates that $\langle \varepsilon \rangle$ is determined from the kinetic energy decay, i.e. (1). For grid turbulence, Taylor's hypothesis is used to transform the time t into a streamwise distance x_1, viz. $\partial x_1 = -U\partial t$. Equation (1) is of considerable importance since $\langle \varepsilon \rangle$ is a quantity that is notoriously difficult to determine in experiments. An additional advantage of HIT is that the transport equation for the two-point velocity correlation function is known exactly for this flow (Kármán and Howarth 1938). The Karman–Howarth equation can be re-expressed in terms of the velocity structure functions (Saffman 1968; Danaila et al. 1999), viz.

$$-\left\langle (\delta_i u_i)^3 \right\rangle = \frac{4}{5}\langle \varepsilon \rangle r_i - 6\nu \frac{\mathrm{d}}{\mathrm{d}r_i}\left\langle (\delta_i u_i)^2 \right\rangle + I_{u_i} \tag{2}$$

where $\langle (\delta_j u_i)^n \rangle \equiv \langle [u_i(x + r_j) - u_i(x)]^n \rangle$, ν is the kinetic viscosity, r_j is a separation vector taken along the x_j-axis, and no summation is implied over indices. In grid turbulence, the streamwise decay is represented by the non-stationary term I_{u_i}, which is expressed as

$$I_{u_i} \equiv -\frac{3U}{r_i^4}\int_0^{r_i} s^4 \frac{\partial}{\partial x_1}\left\langle (\delta_i u_i)^2 \right\rangle \mathrm{d}s, \tag{3}$$

where s is a dummy variable. Expression (2) can be interpreted as a scale-by-scale turbulent energy budget and, as shown below, can be used to quantify the effects of the limited resolution on the different scales of the turbulence.

Concerning the second issue, HWA offers good temporal and spatial resolution, and has been tested extensively in grid turbulence. With suitably chosen experimental conditions, accurate estimates of $\langle \varepsilon \rangle$ as well as the mean enstrophy have been obtained with this method (e.g. Foss and Wallace 1989; Sirivat and Warhaft 1983; Mydlarski and Warhaft 1996; Antonia et al. 1998; Zhou and Antonia 2000b; Zhou et al. 2003; Gagne et al. 2004; Lavoie et al. 2007). It should also be noted that the availability of direct numerical simulations (not only for HIT but also in wall shear flows) has contributed to the development and validations of techniques to correct hot-wire measurements for the effect of finite spatial resolution of the probe (e.g. Suzuki and Kasagi 1992; Antonia 1993; Kim and Antonia 1993; Ewing et al. 1995; Zhu and Antonia 1995; Moin and Mahesh 1998; Antonia et al. 2002). A comparison with HWA can thus be beneficial to assess the ability of PIV (or any other non-intrusive method) to resolve the small-scale motion adequately.

In this paper, PIV and HWA measurements in decaying turbulence behind a woven mesh grid are reported. The first objective is to establish the range of scales over which PIV measurements can be considered reliable (at least for this type of flow) by comparing the two sets of measurements for similar initial conditions. Analytical equations are derived to account for the finite spatial resolution of the PIV, similarly to what has been proposed for HWA (e.g. Wyngaard 1968; Zhu and Antonia 1995, 1996). The effect of resolution on the turbulent kinetic energy, dissipation rate, velocity structure functions and scale-by-scale energy budget are considered. The focus here is on the intermediate-far range ($30 \leq x_1/M \leq 60$, with M the mesh size) where turbulence intensities are low (less than 3%). For the present purpose, the experimental conditions and spatial resolution of each measurement technique have been chosen so that HWA provides adequately resolved measurements, while the resolution of the PIV is purposefully stretched to test its limits in a meaningful manner. This also provides a relatively stringent benchmark against which the effectiveness of the correction method presented in Sect. 2 can be assessed.

2 Experimental details

The PIV tests were performed in the CIRA low speed wind tunnel (CT-1), which is an Eiffel type open circuit wind

tunnel, with the following properties: velocity range from 5–55 m/s, nozzle contraction ratio of 16:1 and a maximum turbulence level of 0.2% at 10 m/s and 0.1% at 50 m/s. The working section was 600 mm long, 302 mm wide and 302 mm high with full optical access. A grid made of woven wires (diameter $d = 1.2$ mm) with mesh size $M = 4.5$ mm was mounted immediately downstream of the contraction, i.e. at the beginning of the working section. The solidity of the grid, $\sigma \equiv d/M(2 - d/M)$, was 0.45 and a Reynolds number, $R_M = UM/\nu$, of 3000 was used (i.e. mean flow velocity $U = 10$ m/s). The pressure gradient in the working section was nearly zero (roughly 1% of the dynamic pressure in the tunnel for $U = 10$ m/s).

A Nd–Yag laser (pulse energy of 300 mJ at a wavelength of 532 nm) was used and images of tracer particles (Di-Sebacate oil with an average diameter of 2 μm) were acquired by a PCO SensiCam at a resolution of 1,280 × 1,024 pixels (12 bit grey level resolution) synchronised with the laser emission (the objective focal length was 100 mm, while the *f*-number was 5.6). Typical images correspond to a region of 80 mm along x_1 and 65 mm along x_2, or about $18M \times 14M$ (the magnification factor was about 15 pixel/mm), while the depth of view was roughly 1 mm due to the laser sheet thickness. This image size was equivalent to roughly five integral length scales and therefore allowed the large scales of the flow to be captured. On an average, the tracer particle size on the images was about three pixels. A time delay (Δt) of around 90 μs, which yielded particle displacements of around 16 pixels at $x/M = 50$, was selected to be optimum based on preliminary investigations. At this location, the turbulence intensity (*TI*) was about 2%, equivalent to a displacement of roughly 0.3 pixels. This provided a dynamic range of about 50; sufficient for capturing the streamwise decay of the turbulence (Poelma et al. 2006). The turbulence intensity further downstream was too low for the PIV to capture the velocity fluctuations (e.g. at $x/M = 100$, *TI* dropped to 1% and the velocity fluctuations were under 0.1 pixels; dynamic range equal to 80). Therefore, the PIV measurements presented here are limited to $x/M \leq 50$. Measurements of the decaying turbulence over a distance greater than 18 *M* were obtained by overlapping acquisition regions along the streamwise direction. Images were processed with the PivView code using standard multi-pass cross-correlations between consecutive images. Interrogation windows (size 32 × 32 pixels, or approximately 2 × 2 mm^2, yielded about 20–25 particles per window) were overlapped over half their width (16 pixels). The selection of this interrogation window size was a result of a compromise between spatial resolution and data quality requirements. Smaller windows significantly increase the number of spurious velocity vectors due to a reduction in the number of particles for each window. Although advanced image deformation algorithms can increase the spatial resolution of PIV (as reported in the results of PIV Challenges 2001, 2003, 2005; see http://www.pivchallenge.org), the present PIV data were obtained without deformation of the interrogation window or of the whole image. This was done for two reasons. First, it gives some general insights for the investigation of a wide range of flow scales with PIV without the use of more advanced algorithms. Second, the sensitivity of PIV to changes in velocity can be simply approximated to be uniformed over the measurement region. This allows the results of the spectral correction analysis (given below) to be more generally applicable. Turbulence statistics were computed over approximately 1,000 images. Homogeneity along the x_2-axis, which was satisfied to within ±1.5% for the mean flow, allowed further averaging of turbulence statistics along the vertical axis. Velocity fluctuations were considered relative to the local mean velocity before averaging to avoid errors due to a possible inhomogeneity of the mean flow.

The HWA measurements were performed in an open circuit wind tunnel at the University of Newcastle. The grid was located immediately downstream of a 9:1 contraction. The working section of the tunnel was 2.4 m long and its square cross-section at the contraction had a width 350 mm. The floor was inclined slightly to provide a zero pressure gradient (the pressure change was less than 0.4% of dynamic pressure in tunnel). The grid used was of the same geometry and wire diameter as for the PIV experiments (woven mesh with $d = 1.2$ mm). However, the mesh size was slightly larger, $M = 5.1$ mm compared to 4.5 mm, which resulted in a grid solidity of $\sigma = 0.42$. Due to the slight difference in mesh length, the mean flow velocity was selected to give the same R_M as for the PIV (i.e. $U = 9.1$ m/s). Lavoie et al. (2007) found that σ only has a very weak effect on the decay and structure of the turbulence. Therefore, the slight difference between the solidities of the woven meshes used in the PIV and HWA experiments does not represent a significant change in initial conditions. The background turbulence intensity for this wind tunnel was about 0.1% at $U = 10$ m/s.

The longitudinal velocity fluctuations were measured with a single wire, while the transverse velocity fluctuations were obtained with a X-wire. All wires had a diameter of 2.5 μm and were etched from Wollaston (Pt-10% Rh) to a length $\ell = 0.5$ mm. The sensors of the X-wire probe were inclined at roughly ±45° relative to the mean flow and separated by a distance of $\Delta x_3 = 0.9$ mm. The wires were operated with in-house constant temperature circuits at an overheat ratio of 0.5. The signals were amplified and low-pass filtered at a cut-off frequency $f_c = 10$ kHz, which corresponded to the onset of electronic noise. The signals were sampled at a frequency $f_s \geq 2f_c$ and

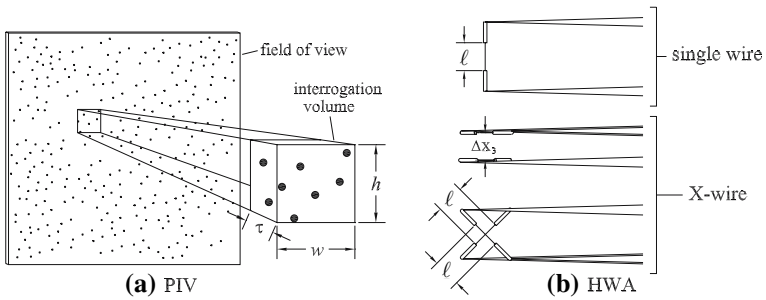

Fig. 1 Schematic illustration of the measurement domain of **a** PIV and **b** HWA (single and X-wire probes are shown)

Table 1 Experimental conditions and spatial resolution for PIV and HWA experiments

	M (mm)	d (mm)	σ	C^*_D	R_M	η (mm)	Resolution
PIV	4.5	1.2	0.45	5.12	3,000	0.15–0.19	$11 \le (h/\eta = w/\eta) \le 14$
							$5 \le \tau/\eta \le 7; 5 \le U\Delta t \le 6$
HWA	5.1	1.2	0.42	4.70	3,000	0.16–0.21	$2.4 \le \ell/\eta \le 3.0$
							$4.3 \le \Delta x_3/\eta \le 5.6$

digitised with a 16 bit A/D converter. The X-wire was calibrated using the look-up table method described by Burattini and Antonia (2005) with 5 angles (±5° in 2.5° increments) and seven velocities between 8 and 10.2 m/s. The single wire was calibrated with standard velocity calibrations (seven velocities between 8 and 10.2 m/s) to which a third-order polynomial was fitted.

Turbulence statistics measured in the laboratory are affected by many sources of uncertainties. Two of these are particularly relevant to the present work. In the first instance, it is important to quantify the statistical convergence of mean quantities. Benedict and Gould (1996) give an extensive discussion on this particular topic and outline expressions to evaluate the variance associated with low- and high-order turbulence statistics. The statistical uncertainty on the mean of variable α (based on a 95% confidence interval) is given by $\pm 1.96(s_\alpha^2/N)^{1/2}$, where s_α^2 is the variance of α and N is the number of independent samples. Recall that for two samples of variable α to be independent, they must be separated by at least twice the integral time (or length) scale of α. In general, each HWA and PIV samples are not independent and thus N must be adjusted to reflect the actual number of integral time (or length) scales included in the total sampling domain. Following the guidelines presented by Benedict and Gould (1996), about 39,200 independent samples are required for $\langle q^2 \rangle$ to converge to within ±1%, while roughly 3 times this amount is required for the negative peak of $\langle (\delta u_i)^3 \rangle$ to converge to ±5%. The present HWA results met these convergence criteria comfortably. For the PIV data, the time between consecutive images was large enough for each image to be independent, while the height of each image corresponded to about ten integral length scales. This yielded 5,000–6,000 independent samples (depending on the streamwise location). As a result, $\langle q^2 \rangle$ converged only to within 3.5–4.0% (this was also evident from the random variations in the measured values of $\langle u_i^2 \rangle$ observed at different y positions at a given x_1/M). This is related to a well known limitation of PIV, viz. the heavy memory and computational costs of acquiring a large number of independent samples in order to achieve adequate statistical uncertainty levels. However, this limitation should become less important with ongoing advances in computer technology.

The second source of errors relates to the limited spatial resolution of the measurement methods used. It is well known that scales smaller than the measurement volume cannot be resolved. This can, in turn, lead to significant errors in the measurements of velocity and velocity derivative statistics. It is therefore important to know the size of the sensing domain of each measurement technique relative to the smallest relevant scale of the flow, viz. the Kolmogorov length scale $\eta (\equiv \nu^{3/4} \langle \varepsilon \rangle^{1/4})$. The sensing domain for PIV is a volume (see Fig. 1) defined by the interrogation window and the thickness of the laser sheet (or in some cases the focal depth of the camera objective). Herein, this domain is referred to as the interrogation volume. This contrasts with the sensing length of a single wire, which can be approximated as a line, or the two inclined wires separated in space by a distance Δx_3 for a X-wire (also shown in Fig. 1). In the case of PIV, the time delay Δt between image pairs must also be considered, since velocity changes within this time cannot be resolved. The dimensions of the measurement domain of PIV and HWA are compared to η in Table 1. Also included in the

table are other important experimental conditions. The relatively coarse resolution of the PIV is somewhat typical of this measurement technique, where the scale resolution is a trade off between zooming the image onto a small area to resolve small scale motion, which can lead to a loss of global information and increases noise (e.g. Saarenrinne and Piirto 2000), and capturing the region of the flow field that includes all relevant scales (e.g. Poelma et al. 2006). This resolution allowed for the PIV performance to be assessed when its capabilities are being stretched and made it possible to test the correction procedure presented herein. However, we note, for reference, that Poelma et al. (2006) have reported PIV measurements for grid turbulence at $R_\lambda = 25$ in water obtained with an interrogation window size of approximately $3\eta \times 3\eta$ with $U\Delta t = 4\eta$ (laser sheet thickness was unspecified).

Means of estimating the bias errors associated with finite spatial resolution of HWA are described by Wyngaard (1968) and Zhu and Antonia (1996). Here this approach is extended to PIV. We assumed that the instantaneous velocity measured with PIV at a given point x_o is the average of the velocity field inside the measurement volume, so that

$$u_i^M(\boldsymbol{x}_o) = \frac{1}{\tau h w \Delta t} \int_{-\Delta t/2}^{\Delta t/2} \int_{-\tau/2}^{\tau/2} \int_{-h/2}^{h/2} \int_{-w/2}^{w/2} u_i(\boldsymbol{x}_o + \boldsymbol{s}, t)\, \mathrm{d}\boldsymbol{s}\, \mathrm{d}t, \tag{4}$$

where $\boldsymbol{s}$ is a dummy 3D vector that defines the interrogation volume, $\boldsymbol{x}_o$ is at the centre of the domain and the superscript M indicates the measured velocity. Equation (4) is based on the assumption that the sensitivity of the interrogation volume to the velocity field is the same (on average) throughout its domain, which is a simplified approach. However, the procedure described can be generalised by introducing an analytic weighted average in (4) that may be more representative of the sensitivity of the interrogation domain in particular flows (e.g. with high velocity gradients) or when more specialised procedures are used to infer the velocity field from PIV images (e.g. Nogueira et al. 1999).

We can represent the velocity field, if it is assumed to be homogeneous, by the Fourier-Stieltjes integral (Batchelor 1953), viz.

$$u_i(\boldsymbol{x}) = \int_{-\infty}^{\infty} e^{j\boldsymbol{k}\cdot\boldsymbol{x}}\, \mathrm{d}Z_i(\boldsymbol{k}), \tag{5}$$

where $j \equiv \sqrt{-1}$ and $\boldsymbol{k}$ is the wavenumber vector. Equation (4) can be rearranged, by making use of (5), to give

$$u_i^M(\boldsymbol{x}_o) = \int_{-\infty}^{\infty} \left[\frac{1}{U\Delta t} \int_{-U\Delta t/2}^{U\Delta t/2} \left(\frac{1}{\tau h w} \int_{-\tau/2}^{\tau/2} \int_{-h/2}^{h/2} \int_{-w/2}^{w/2} e^{j\boldsymbol{k}\cdot\boldsymbol{s}} \mathrm{d}\boldsymbol{s} \right) e^{jU\Delta t k_1} \mathrm{d}(Ut) \right] e^{j\boldsymbol{k}\cdot\boldsymbol{x}} \mathrm{d}Z_i(\boldsymbol{k}), \tag{6}$$

where Taylor's hypothesis was invoke to project the time axis onto the Δx_1-axis; that is to say, the information about the particles trajectory that is lost due to the finite time difference between expositions is handled as a spatial filter of length $\Delta x_1 = -U\Delta t$[1]. An expression relating the true and measured Fourier-Stieltjes components can be derived from (6), which takes the following form

$$\mathrm{d}Z_i^M(\boldsymbol{k}) = A\, \mathrm{d}Z_i(\boldsymbol{k}), \tag{7}$$

where A is the spectral filtering function that represents the effect of finite resolution averaging. For PIV, this filtering function is given by

$$A = \frac{16}{(wk_1)(U\Delta t k_1)(hk_2)(\tau k_3)} \sin\left(\frac{k_1 w}{2}\right) \sin\left(\frac{k_1 U\Delta t}{2}\right) \sin\left(\frac{k_2 h}{2}\right) \sin\left(\frac{k_3 \tau}{2}\right). \tag{8}$$

Expression (7) is of the same form as that derived by Wyngaard (1968) for a single wire, for which case, the spectral filtering function is

$$A = \frac{\sin(\ell k_3/2)}{\ell k_3/2}, \tag{9}$$

where the single wire is taken to be aligned along x_3. The true and measured spectral density tensors (Batchelor 1953) are defined as

$$\Phi_{ii}(\boldsymbol{k})\, \mathrm{d}\boldsymbol{k} = \left\langle \mathrm{d}Z_i(\boldsymbol{k})\, \mathrm{d}Z_i^*(\boldsymbol{k}) \right\rangle \tag{10}$$

[1] Strictly speaking, the displacement of particles over a period Δt is a Lagrangian phenomenon, while Taylor's hypothesis is a Eulerian concept. However, these two frameworks are equivalent in the limit $\Delta t \to 0$, and thus, this assumption is adequate for the purposes of the correction method.

$$\Phi_{ii}^{M}(\boldsymbol{k})\mathrm{d}\boldsymbol{k} = \left\langle \mathrm{d}Z_i^{M}(\boldsymbol{k})\,\mathrm{d}Z_i^{M*}(\boldsymbol{k})\right\rangle, \tag{11}$$

where the asterisk denotes a complex conjugate. It thus follows that

$$\Phi_{ii}^{M}(\boldsymbol{k}) = A^2\Phi_{ii}(\boldsymbol{k}). \tag{12}$$

The same can be applied to the spectra of the velocity derivatives $\langle(\partial u_i/\partial x_n)^2\rangle$, which yields

$$\Phi_{i,n}^{M}(\boldsymbol{k}) = \frac{\sin^2(\Delta x_n k_n/2)}{(\Delta x_n/2)^2}\Phi_{ii}^{M}(\boldsymbol{k}), \tag{13}$$

where Δx_n is the distance between each independently measured values of u_i (i.e. values that are obtained from non-overlapping windows) along the direction x_n. This form of (13) is general and can be applied to any measurement method for which $\Phi_{ii}^{M}(\boldsymbol{k})$ is known.

Correction ratios for one-dimensional velocity spectra are defined as

$$R_{u_i}(k_1) = \frac{\phi_{u_i}^{M}(k_1)}{\phi_{u_i}(k_1)} = \frac{\int\int_{-\infty}^{+\infty}\Phi_{ii}^{M}(\boldsymbol{k})\mathrm{d}k_2\mathrm{d}k_3}{\int\int_{-\infty}^{+\infty}\Phi_{ii}(\boldsymbol{k})\mathrm{d}k_2\mathrm{d}k_3}, \tag{14}$$

where the 'true' spectra $\Phi_{ij}(\boldsymbol{k})$ for isotropic turbulence are given by (e.g. Batchelor 1953)

$$\Phi_{ij}(\boldsymbol{k}) = \Phi_{ij}(k) = \frac{E(k)}{4\pi k^4}\left(k^2\delta_{ij} - k_i k_j\right), \tag{15}$$

k is the magnitude of $\boldsymbol{k}$, $E(k)$ is the 3D energy spectrum and δ_{ij} is the Kronecker delta. Similarly, correction coefficients for the components of the mean turbulent kinetic energy and vorticity variance are defined as

$$r_{u_i} = \frac{\langle u_i^2\rangle^{M}}{\langle u_i^2\rangle} = \frac{\int\int\int_{-\infty}^{+\infty}\Phi_{ii}^{M}(\boldsymbol{k})\mathrm{d}k_1\mathrm{d}k_2\mathrm{d}k_3}{\int\int\int_{-\infty}^{+\infty}\Phi_{ii}(\boldsymbol{k})\mathrm{d}k_1\mathrm{d}k_2\mathrm{d}k_3} \tag{16}$$

$$r_{u_{i,n}} = \frac{\left\langle(\partial u_i/\partial x_n)^2\right\rangle^{M}}{\left\langle(\partial u_i/\partial x_n)^2\right\rangle} = \frac{\int\int\int_{-\infty}^{+\infty}\Phi_{i,n}^{M}(\boldsymbol{k})\mathrm{d}k_1\mathrm{d}k_2\mathrm{d}k_3}{\int\int\int_{-\infty}^{+\infty}\Phi_{i,n}(\boldsymbol{k})\mathrm{d}k_1\mathrm{d}k_2\mathrm{d}k_3}, \tag{17}$$

where the true velocity derivative spectra are given by $\Phi_{i,n}(\boldsymbol{k}) = k_n^2\Phi_{ii}(\boldsymbol{k})$.

The correction coefficients for velocity and velocity derivative statistics can be calculated from (12)–(17) with the spatial filtering function expressed by either (8) or (9), provided $E(k)$ is known. For the results presented in this paper, the correction coefficients were calculated using the 3D spectra $E(k)$ obtained from the DNS of HIT by Antonia and Orlandi (2004). For comparison, Figs. 2 and 3 show the correction ratios R_{u_i} and correction coefficients r_{u_i} and $r_{u_{i,n}}$ estimated for different sensor resolutions. The PIV results presented in the figures are for a square interrogation window ($h = w$) with a laser sheet thickness $\tau = h/2$, while Δt is neglected for simplicity. Figure 2 illustrates the range of scales affected by spatial resolution and shows that the volume averaging of PIV causes a more significant attenuation of the spectra at high wavenumbers compared to a HWA probe with similar sensing dimensions. For example, the small scales ($k_1\eta > 0.5$) are more closely represented by a single hot-wire with $\ell = 8\eta$ compared to a PIV interrogation volume with $h = \ell/2$. Even when compared to a X-wire probe, which could be argued to average the velocity over a sensing domain resembling a volume, the spectral attenuation of PIV is only marginally improved for the case where the X-wire dimensions are twice that for the PIV (Fig. 2). The results presented in Fig. 3 show how the spectral attenuation of the volume averaging for PIV affects the integral quantities $\langle u_i^2\rangle$ and $\langle(\partial u_i/\partial x_n)^2\rangle$. It is perhaps not surprising that the corrections to these quantities are not as significant for PIV as might be suggested from Fig. 2, particularly in the case of $\langle u_i^2\rangle$, since most of the turbulent energy is typically located at scales of the order of the integral length scale, which is roughly equal to 20η for $R_\lambda \sim 40$. At such scales, the difference in the ratio R_{u_i} between PIV and HWA is much less important. On the other hand, because $\langle(\partial u_i/\partial x_n)^2\rangle$ is more heavily weighted towards the small scales of the flow, the difference in the correction coefficient $r_{u_{i,n}}$ between HWA and PIV is larger than that for r_{u_i}.

Before concluding this section, it is relevant to discuss the main drawback of the correction method described above, viz. the requirement that the velocity spectra be known a priori. Of course, any method for estimating the error associated with spatial resolution requires some

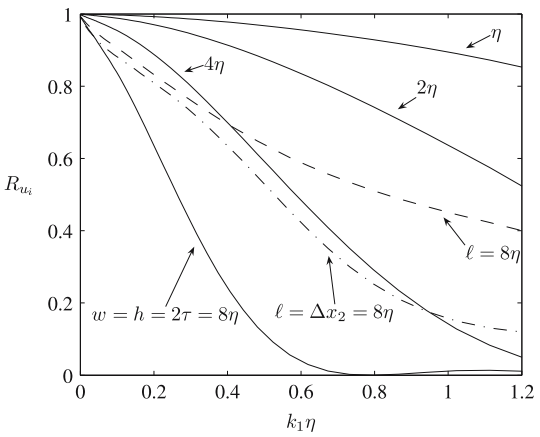

Fig. 2 Spectral correction ratio R_{u_i} for PIV at different spatial resolutions (*solid lines*); the relative dimensions of the interrogation volume are assumed to be $h = w = 2\tau$. Also included for comparison are the ratios $R_{u_i}(i = 1)$ for a single hot-wire ($\ell = 8\eta$; *dash line*) and a X-wire ($\ell = \Delta x_2 = 8\eta$; *broken line with dots*)

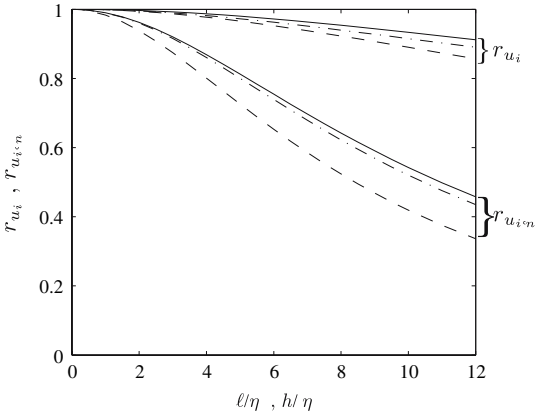

Fig. 3 Correction coefficients R_{u_i} and $r_{u_{i,n}}$ for a single hot-wire of length ℓ (*solid line*), X-wire with probe dimensions $\Delta x_3 = \ell$ (*broken line with dots*) and PIV with interrogation volume given by $h \times h$ and $\tau = h/2$ (*dash line*). Δx_n is taken equal to ℓ for HWA and h for PIV

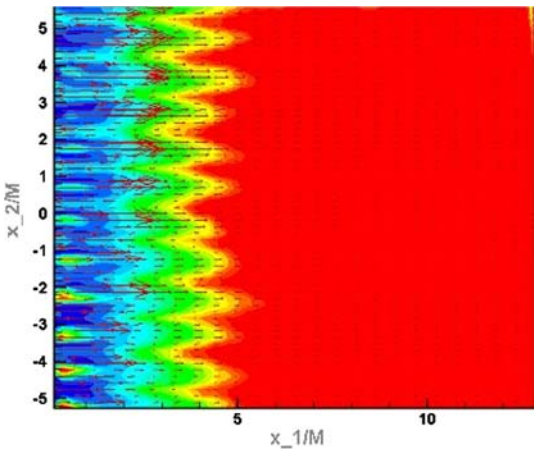

Fig. 4 Evolution of $\langle u_1^2 \rangle / U^2$ (*colour contours*) measured with PIV near the grid ($x_1/M = 0$ corresponds to the location of the grid). Regions of high and low turbulence energy are in *blue* and *red*, respectively. The mean velocity field is represented by the *red arrows*

knowledge of the flow field that acts over the measurement volume of the sensor. Given that the impact of a limited spatial resolution is much more significant at the smaller scales of the flow, the shape of the model used for $E(k)$ at the high wavenumbers will have the most effect on the computed corrections. Since the small scales can be considered to have nominally universal characteristics for moderate to large Reynolds numbers, one can use a variety of semi-empirical models for $E(k)$ to yield good estimates of the error due to spatial resolution (Ewing et al. 1995; Zhu and Antonia 1995). Alternatively, it is possible to use $E(k)$ (normalised with Kolmogorov variables) measured in the same flow at a lower value of R_λ, for which the small scales can be properly resolved (Zhu and Antonia 1996). These assumptions have been tested in some detail previously and were found to be adequate (see for example Kim and Antonia 1993; Zhu and Antonia 1996).

3 Turbulence decay

The turbulent velocity field close to the grid is shown in Fig. 4, where the rms values of the longitudinal velocity u_1 measured via PIV are plotted. Regions of high and low turbulence intensity, associated with individual wakes from the grid elements, are clearly visible for $x_1/M < 5$. As these wakes merge further downstream, the flow approaches homogeneity in the transverse direction for roughly $x_1/M > 10$. This figure illustrates the evolution of the turbulence from a highly non-homogeneous velocity field close to the grid, where it is generated, to a state where it becomes homogeneous and isotropic to a close approximation. Figure 4 highlights one of the attractive advantages of PIV, which is its potential to study complex flow fields as a whole, since it provides simultaneous velocity vectors at many different spatial locations. This is particularly important when studying the large scales of turbulence and their dynamics. Of course, it would be extremely difficult, if not entirely impractical, to obtain such detailed measurements of the flow field with HWA, particularly immediately downstream of the grid, where the turbulence intensity is very high and flow reversal occurs.

In order to compare the turbulent kinetic energy obtained from HWA and PIV, $\langle q^2 \rangle$ must be normalised to account for the slight difference in the solidity of the grids used in each experiment. Batchelor and Townsend (1948) showed that $\langle q^2 \rangle$ at a given distance downstream of grids is proportional to the pressure drop coefficient of the grid C_D. Given that for woven mesh grids (Laws and Livesey 1978)

$$C_D = B \frac{1 - (1 - \sigma^2)}{\sigma(1 - \sigma^2)} \equiv C_D^*, \tag{18}$$

where B is a constant of proportionality and C_D^* is an intermediate variable defined here to simplify the presentation of the data, it follows that $\langle q^2 \rangle / U^2 C_D^*$ should collapse the curves for both grids. The value of C_D^* appropriate to each experimental setup is reported in Table 1.

Figure 5 shows the streamwise decay of $\langle q^2 \rangle / U^2 C_D^*$ obtained with HWA and PIV. Here, $\langle q^2 \rangle$ is assumed equal to $\langle u_1^2 \rangle + 2\langle u_2^2 \rangle$, since this flow satisfies axisymmetry relative to the streamwise direction (i.e. it is invariant to rotations with respect to x_1). Both corrected and uncorrected data for PIV are shown in the figure, while the uncorrected HWA data have not been included since they are indistinguishable from the corrected ones. The uncorrected data for the PIV is significantly underestimated (by roughly 20%), as expected due to the coarser resolution of

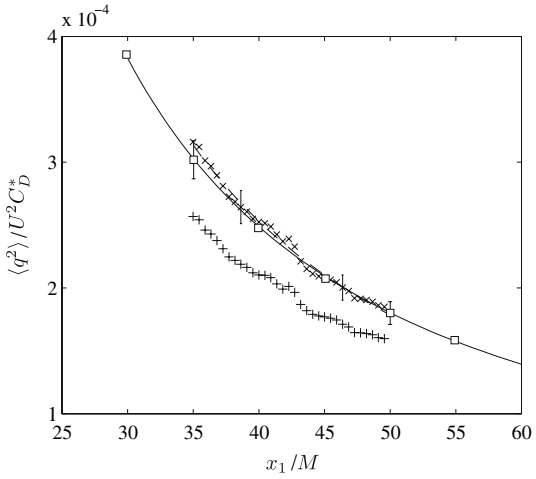

Fig. 5 Streamwise evolution of $\langle q^2\rangle/U^2C_D^*$ measured with HWA (corrected: *square*) and PIV (uncorrected: *plus sign*; corrected: *multi sign*), and associated power-law (HWA: *solid line*; PIV: *dash line*). For clarity, only every second point is shown for the PIV. Error bars indicate experimental uncertainties for HWA and PIV data

the PIV. However, once corrected, the PIV results are virtually identical to the HWA measurements, which shows that the turbulent kinetic energy can be estimated accurately with the latter even when the small-scale resolution is relatively poor. Further, we note that the limited statistical convergence of the PIV data can be inferred from the significantly larger scatter in the data compared to HWA.

Predictions about the decay of HIT based on self-similarity yield the well known power-law decay of turbulence (Batchelor and Townsend 1948; George 1992), viz.

$$\frac{\langle q^2\rangle}{U^2} = A\left(\frac{x_1}{M} - \frac{x_o}{M}\right)^m, \tag{19}$$

where m is the power-law exponent, x_o is a virtual origin and A is a constant of proportionality. The power-laws obtained with a non-linear least-squares regression of (19) to the corrected PIV and HWA data are also included in Fig. 5. The values for the power-law exponents obtained are $m = -1.28$ and -1.38 for the HWA and PIV measurements, respectively. These estimates of m are accurate to ± 0.1, where the high level of uncertainty is due to the small number of measurements available for the HWA and large scatter in the PIV. Nonetheless, the present values of m are in good agreement with those found in the literature (e.g. Comte-Bellot and Corrsin 1966; George 1992; Lavoie et al. 2007), while the results obtained with both HWA and PIV are within experimental uncertainty.

Reliable estimates of the dissipation rate $\langle\varepsilon\rangle_d$ can be obtained by introducing (19) into (1) and differentiating with respect to x_1 to yield

$$\langle\varepsilon\rangle_d = -\frac{AmU}{2M}\left(\frac{x_1}{M} - \frac{x_o}{M}\right)^{m-1}. \tag{20}$$

The values of $\langle\varepsilon\rangle_d$ obtained from (20) are shown in Fig. 6 for both HWA and PIV. As suggested by the results shown in Fig. 5, $\langle\varepsilon\rangle_d$ is significantly underestimated from the uncorrected PIV data. However, the agreement between the values of the dissipation obtained with the corrected results of PIV and those of HWA is significantly improved.

Assuming local isotropy, $\langle\varepsilon\rangle$ can be simply estimated from the mean square value of the streamwise velocity derivative via (e.g. Tennekes and Lumley 1972)

$$\langle\varepsilon\rangle_{\rm iso} = 15\nu\left\langle\left(\frac{\partial u_1}{\partial x_1}\right)^2\right\rangle, \tag{21}$$

where the subscript iso indicates that it is an isotropic approximation of the true $\langle\varepsilon\rangle$. Figure 7 compares the measured values of $\langle\varepsilon\rangle_{\rm iso}$ to $\langle\varepsilon\rangle_d$ for both measurement methods. Due to the relatively coarse resolution of the present PIV measurements, the uncorrected data yield values of $\langle\varepsilon\rangle_{\rm iso}$ about 75% lower than $\langle\varepsilon\rangle_d$. Once corrected, the PIV data are in very good agreement with the HWA results, although they remain roughly 15% below the values for $\langle\varepsilon\rangle_d$. Note that the HWA results obtained with (21) are also lower than the mean energy dissipation rate estimated from (20) by roughly 10%. This difference is common in grid turbulence (e.g. Zhou and Antonia 2000a) and is due to possible small deviations from isotropy at the small scales as well as experimental errors (typically, uncertainties on estimates of $\langle(\partial u_1/\partial x_1)^2\rangle$ are

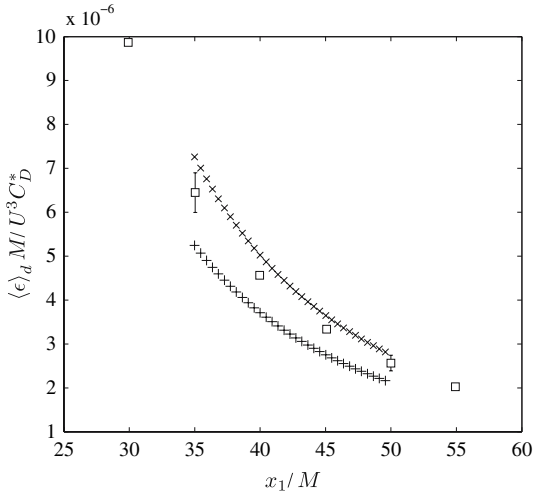

Fig. 6 Normalised turbulence energy dissipation rate measured from (20) with HWA (corrected: *square*) and PIV (uncorrected: *plus sign*; corrected: *multi sign*) data. For clarity, only every second point is shown for the PIV. Error bars indicate experimental uncertainties for HWA data

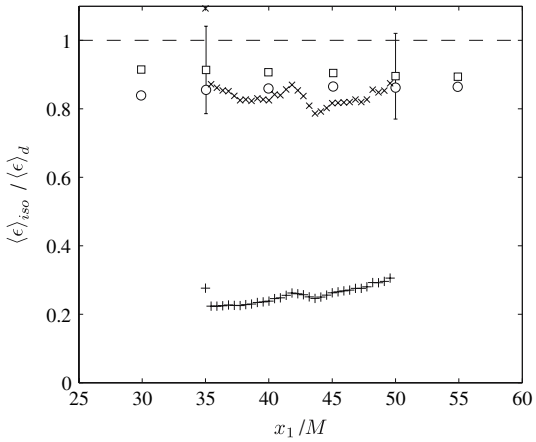

Fig. 7 Ratio $\langle\varepsilon\rangle_{iso}/\langle\varepsilon\rangle_d$ measured with HWA (uncorrected: *circle*; corrected: *square*) and PIV (uncorrected: *plus sign*; corrected: *multi sign*). For clarity, only every second point is shown for the PIV. Error bars indicate experimental uncertainties for HWA data

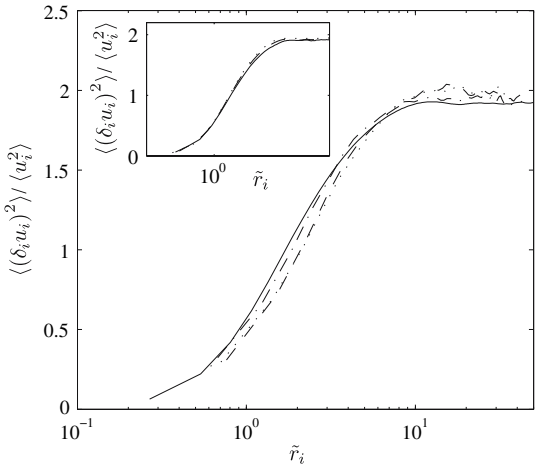

Fig. 8 Second-order structure functions measured with a single HWA (i = 1: *solid line*) at x_1/M = 45 and PIV (i = 2) at x_1/M = 36 (*broken line*), 41 (*dotted line*) and 50 (*broken line with dots*). The inset compares the functions measured with HWA at x_1/M = 35, 45 and 55

~10–15%). As mentioned earlier, the present experimental conditions are stretching the ability of the PIV to resolve the turbulence and it is therefore to be expected that the small scales should not be adequately captured in this case—particularly, the uncorrected results. Nonetheless, it is encouraging to note that, although the magnitude of the PIV corrections is large, the corrected values are within experimental uncertainties of the corrected HWA data.

4 Velocity structure functions

In order to compare the longitudinal structure functions $\langle(\delta_i u_i)^n\rangle$ measured with PIV and HWA, these must be evaluated with separation vectors taken along a direction where the turbulence is homogeneous. In the case of HWA, each measurement is separated by a time Δt and Taylor's hypothesis is used to give a separation vector r_1 (i.e. $r_1 = -U\Delta t$). For a steady flow, homogeneity along r_1 is satisfied by definition. For PIV, the direction transverse to the mean flow is homogeneous, so that i = 2 is used for this case.

The second-order longitudinal structure functions measured at three downstream positions with PIV are compared with those obtained at x_1/M = 45 with HWA in Fig. 8. The structure functions here are normalised in accordance with the equilibrium similarity postulate of George (1992), viz.

$$\left\langle(\delta_i u_i)^2\right\rangle = \langle u_i^2\rangle f_i(\tilde{r}_i) \tag{22}$$

$$-\left\langle(\delta_i u_i)^3\right\rangle = \left[\frac{\langle u_i^2\rangle^{3/2}}{R_\lambda}\right] g_i(\tilde{r}_i), \tag{23}$$

where a tilde represents normalisation with the Taylor microscale, $\lambda = (15\nu\langle u_1^2\rangle/\langle\varepsilon\rangle)^{1/2}$, and $R_\lambda = \langle u_1^2\rangle^{1/2}\lambda/\nu$ is the Taylor microscale Reynolds number. The inset of Fig. 8 demonstrates that the structure functions are nearly independent of the downstream location for the HWA (i.e. the decay of the turbulence is approximately self-similar). Although the PIV data are generally lower than the HWA data at small $\tilde{r}_1$, due to spatial resolution effects, they are in reasonable agreement with each other. It is also important to note that the structure functions, as obtained by both methods, are nearly identical in shape, even at large separations, implying that Taylor's hypothesis does not have a strong influence on the shape of these functions—at least in this flow, where the turbulence intensity is low. (The small undulations at large $\tilde{r}$ for the PIV data are due to the poor statistical convergence and do not reflect the structure of the large scales.)

In Fig. 9, the third-order longitudinal structure functions, divided by $\tilde{r}_i$, that were measured with PIV are compared to those obtained at x_1/M = 45 with HWA. The agreement between HWA and PIV data is not as good as for the second-order structure function data. In particular, the peak of $-\langle(\delta_i u_i)^3\rangle/\tilde{r}_i$ is greatly underestimated for PIV. This is perhaps not surprising given that higher order functions are more sensitive to the spatial resolution. As an illustration, the inset of Fig. 9 shows results obtained by undersampling one of the HWA signals in order to mimic a coarser resolution. A sampling frequency N times smaller than f_s, where N is a positive integer, can be simulated by using only every Nth data point in the original time series. The spatial averaging of the PIV along x_1 can be accounted for when the velocity at time t is taken as the average of the velocities

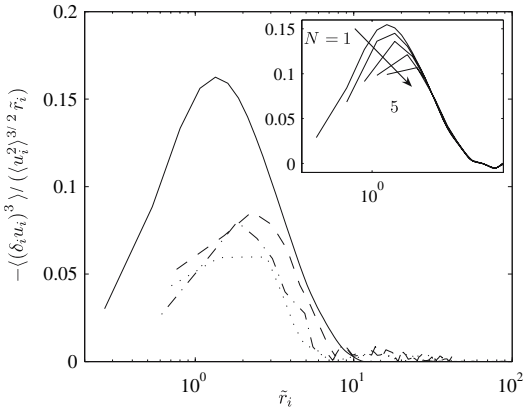

Fig. 9 Third-order structure functions measured with a single HWA (i = 1: *solid line*) at x_1/M = 45 and PIV i = 2 at x_1/M = 36 (*broken line*), 41 (*dotted line*) and 50 (*broken line with dots*). The inset shows the result of undersampling the HWA signal obtained at x_1/M = 45 with a frequency N times smaller than the actual sampling frequency

measured over $t \pm N/f_s$. This procedure also incorporates the overlap between interrogation windows, although the averaging in the x_2 and x_3 directions due to the interrogation volume of PIV cannot be included. The curve for N = 5, which represents an averaging domain of about 11η (similar to the resolution of the PIV), bears a close resemblance to the PIV results. Figure 9 demonstrates that for the magnitude of the peak in $-\langle(\delta_i u_i)^3\rangle/\tilde{r}_i$ to be properly determined, a sensing resolution several times smaller than λ, the approximate location of the peak, is required. This would represent an interrogation volume smaller than $\sim(5\eta)^3$ for the present experimental conditions.

Some of the difficulties in evaluating the non-stationary term in (2) can be alleviated by making use of the fact that the turbulence decays in an approximately self-similar manner, as was demonstrated in the inset of Fig. 8. The similarity form of (2) can then be expressed as (Lavoie et al. 2005)

$$g_i + 6f_i' - \left[\frac{15\Gamma_{u_i1}}{m} - 30\Gamma_{u_i2}\right]\tilde{r}_i^{-4} = 12\tilde{r}_i, \tag{24}$$

where the prime denotes differentiation with respect to $\tilde{r}_i$, while Γ_{u_i1} and Γ_{u_i2} are given by

$$\Gamma_{u_i1} \equiv \int_0^{\tilde{r}_i} \tilde{s}^5 f_i' \,\mathrm{d}\tilde{s} \tag{25}$$

$$\Gamma_{u_i2} \equiv \int_0^{\tilde{r}_i} \tilde{s}^4 f_i \mathrm{d}\tilde{s}. \tag{26}$$

While the first and second terms on the left-hand side of (24) represent the non-linear energy transfer and dissipation rates, respectively, the term in the square brackets ($\tilde{I}_{u_i}$) is the non-stationary component due to the streamwise

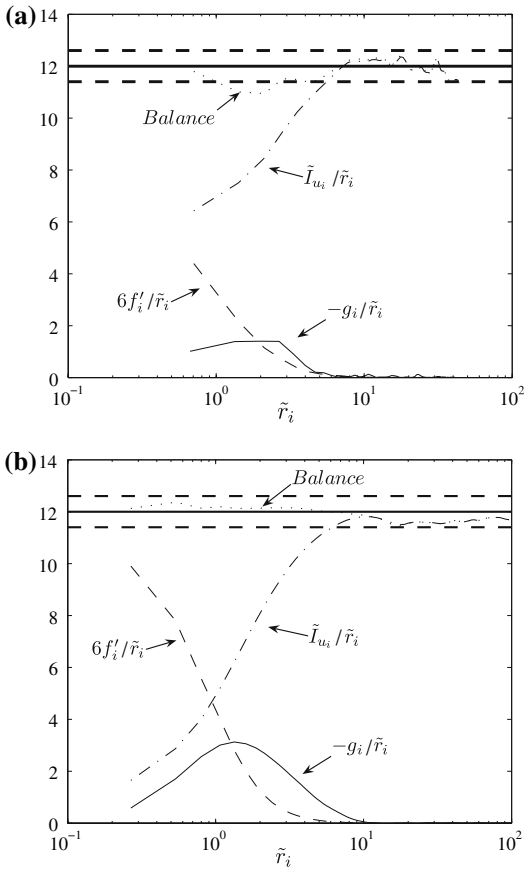

Fig. 10 Scale-by-scale energy budget given by (24) and measured with **a** a single HWA at x_1/M = 45 (i = 1) and **b** PIV at $x_1/M = 41 (i = 2)$. $-g_i/\tilde{r}_i$, *solid line*; $6f_i'/\tilde{r}_i$, *broken line*; $\tilde{I}_{u_i}/\tilde{r}_i$, *broken line with dots*; left hand side balance of (23), *dotted line*. The *thick horizontal line* is at 12 (±5%, *thick horizontal dash lines*)

decay of the turbulence. Each term in (24) was computed for both the HWA and PIV data and is shown in Fig. 10. Only one downstream location is shown since similar results were obtained at other x_1/M. Equation (24) is well balanced at all scales for the HWA data in Fig. 10(a) (differences between the sums of the terms on the right and left hand sides are within ±5%). Despite the poor resolution for the PIV, (24) appears relatively well balanced at all separations. However, the results of Figs. 8 and 9 suggest that the energy transfer and dissipation terms in (24) are in fact significantly underestimated at small separations ($\tilde{r}_i < 2$). The apparent balance of the scale-by-scale energy budget can be accounted for by the behaviour of the non-stationary term $\tilde{I}_{u_i}$, which is shown in Fig. 11. Although the magnitude of $\tilde{I}_{u_i}$ at large values of $\tilde{r}_i$ is nearly identical for both measurement techniques, the poor resolution at small scales for the PIV data causes the term $f_i'(\tilde{r}_i)$ in (25) to be significantly overestimated. The effect of poor spatial resolution is further illustrated in the inset of Fig. 11, where the results obtained by undersampling a HWA signal are shown. When N is increased, these curves display a similar

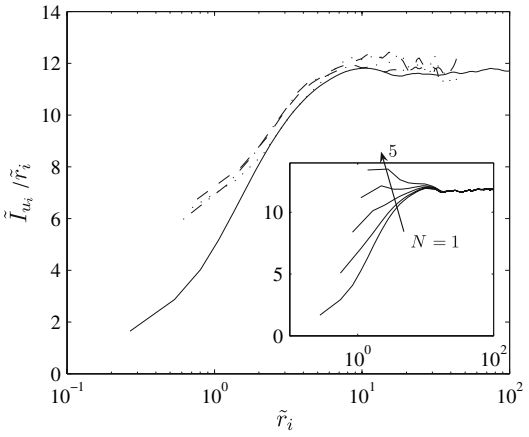

Fig. 11 Comparison of the non-stationary term $\tilde{I}_{u_i}$ measured with a single HWA ($i = 1$) at $x/M = 45$ (*solid line*) and PIV ($i = 2$) at $x/M = 36$ (*broken line*), 41 (*dotted line*) and 50 (*broken line with dots*). The inset shows the result of undersampling the HWA signal obtained at $x_1/M = 45$ with a frequency N times smaller than the actual sampling frequency

trend to that found in the PIV results. The overestimation of I_{u_i} at small $\tilde{r}_i$ thus seems to compensate for the overestimation of the other terms on the left-hand side of (24).

5 Conclusions

The spatial resolution of HWA and PIV data relative to the smallest scales of a turbulent flow is an important factor which can impose considerable limitations on the accuracy of the measurements in such flows. For the present flow conditions, the HWA had a resolution roughly 4 times better than that of PIV (about 2–4η for HWA and 11–14η for PIV). The results obtained from both measurement techniques were compared in order to study the effect of the finite spatial resolution of PIV on turbulence statistics. The discussion was further supported by the use of an analytical method—similar to that applied to HWA data—to account for the effect of finite resolution on PIV data. The results show that for a PIV interrogation volume of dimensions equal to a given hot-wire size, the attenuation of the velocity and velocity derivative statistics is significantly larger for the former, due to the volume averaging associated with PIV. This assessment of the finite resolution effects is exclusive of any other sources of errors associated with either measurement method.

The uncorrected PIV measurements of the turbulent kinetic energy are significantly underestimated due to poor spatial resolution. However, even for the stringent conditions designed for this study, the correction method compensates for the attenuation of velocity fluctuations due to finite resolution. As a result, the corrected PIV results are in close agreement with the HWA data. Nonetheless, the spatial resolution of the PIV for the present experimental conditions is not sufficient to estimate the velocity derivative statistics with confidence. It is suggested that an interrogation window of width less than or equal to 5η with a laser sheet half this dimension in thickness would be required for the small scale statistics to be estimated with acceptable accuracy (corrections of less than 30% are required at this resolution). This dimension is similar to the resolution that has previously been suggested for hot-wire arrays (e.g. Zhu and Antonia 1995; Zhou et al. 2003).

The second-order velocity structure functions $\langle(\delta_i u_i)^2\rangle$ measured with PIV and HWA are in close agreement with each other, notwithstanding a slight reduction in the PIV data arising from the coarser resolution. The lack of significant differences in the shape of the structure functions at large separation suggests that the approximation due to Taylor's hypothesis, required to yield $\langle(\delta_1 u_i)^2\rangle$ in the case of HWA, is not important for this flow where the turbulence intensity is low (<5%). The third-order structure functions are more sensitive to the limited spatial resolution of the measurement method and thus display larger deviations between the two measurement methods. In particular, the peak magnitude of $\langle(\delta_i u_i)^3\rangle/r_i$ is largely underestimated by the PIV. This has obvious implications for PIV-based investigations in the so-called ''scaling range''. The agreement between PIV and HWA for the third-order structure functions is reasonable only at large separations ($r/\lambda > 3$, i.e. more than 6 times the PIV resolution). Despite the third-order structure functions being significantly underestimated, the balance of the scale-by-scale budget, given by the transport equation of $\langle(\delta_i u_i)^2\rangle$, is fairly good for the PIV. The balance is retrieved due to errors associated with the non-stationary term, which is overestimated because of the poor resolution of $\langle(\delta_i u_i)^2\rangle$ with respect to r_i. It is important to be aware of this limitation since this apparent lack of sensitivity of the scale-by-scale budget to measurement resolution may lead to an erroneous interpretation of experimental results.

Overall, this work confirms the relevance of HWA for studying turbulent flows whilst highlighting the advantages offered by PIV, such as the availability of simultaneous velocity measurements at numerous points in space. To obtain such measurements with HWA would require multiple sensors that may impose a significant blockage to the flow. It also illustrates the importance of a number of issues that need to be considered carefully when designing experiments. In particular, the spatial resolution should be selected carefully if all the turbulent scales of interest (largest and smallest) are to be evaluated correctly. Given a particular camera resolution, a compromise needs to be found between an image size large enough to capture the large scales and an interrogation window small enough to

capture the small scales, while still providing an appropriate signal to noise ratio to minimise the number of spurious velocity vectors. In addition, given the computational expense of storing and processing large numbers of PIV images, statistical tools should be used for optimising the number of images required to achieve the desired statistical convergence for the flow parameters of interest. These issues are not new and have to be handled by researchers interested in turbulent flows. However, their importance cannot be understated and warrants constant vigilance by experimentalists; particularly with the growing availability of measurement systems in the form of streamlined user friendly black boxes. Nevertheless, it is encouraging to note that the typical resolution of current PIV measurements is constantly improving due to the continuing advances in technology, and data acquisition and processing techniques.

Acknowledgements We thank Drs. R.J. Smalley and P. Burattini for many useful discussions. PL and RAA acknowledge the support of the Australian Research Council.

References

Antonia RA (1993) Direct numerical simulations and hot wire experiments: a possible way ahead? In: Dracos T, Tsinober A (eds) New approaches and concepts in turbulence. Birkhäuser Verlag, Basel, pp 349–365

Antonia RA, Orlandi P (2004) Similarity of decaying isotropic turbulence with a passive scalar. J Fluid Mech 505:123–151

Antonia RA, Zhou T, Zhu Y (1998) Three-component vorticity measurements in a turbulent grid flow. J Fluid Mech 374:29–57

Antonia RA, Orlandi P, Zhou T (2002) Assessment of a three-component vorticity probe in decaying turbulence. Exp Fluids 33:384–390

Antonia RA, Smalley RJ, Zhou T, Anselmet F, Danaila L (2003) Similarity of energy structure functions in decaying homogeneous isotropic turbulence. J Fluid Mech 487:245–269

Batchelor GK (1953) The theory of homogeneous turbulence. Cambridge University Press, London

Batchelor GK, Townsend AA (1947) Decay of vorticity in isotropic turbulence. Proc R Soc London Ser A 190: 534–550

Batchelor GK, Townsend AA (1948) Decay of isotropic turbulence in the initial period. Proc R Soc London Ser A 193: 539–558

Benedict LH, Gould RD (1996) Towards better uncertainty estimates for turbulence statistics. Exp Fluids 22:129–136

Burattini P, Antonia RA (2005) The effect of different X-wire calibration schemes on some turbulence statistics. Exp Fluids 38:80–89

Comte-Bellot G, Corrsin S (1966) The use of a contraction to improve the isotropy of grid-generated turbulence. J Fluid Mech 25:657–682

Corrsin S (1963) Turbulence: experimental methods. In: Függe S, Truesdell CA (eds) Handbuch der Physik. Springer, Heidelberg, pp 524–589

Danaila L, Anselmet F, Zhou T, Antonia RA (1999) A generalisation of Yaglom's equation which accounts for the large-scale forcing in heated decaying turbulence. J Fluid Mech 391:359–372

Ewing D, Hussein HJ, George WK (1995) Spatial resolution of parallel hot-wire probes for derivative measurements. Exp Therm Fluid Sci 11:155–173

Foss JF, Wallace JM (1989) The measurement of vorticity in transitional and fully developed turbulent flows. In: Gad-el-Hak M (ed) Lecture notes in engineering, vol 45. Springer, Heidelberg, pp 263–321

Foucaut JM, Carlier J and Stanislas M (2004) PIV optimization for the study of turbulent flow using spectral analysis. Meas Sci Technol 15:1046–1058

Gagne Y, Castaing B, Baudet C, Malécot Y (2004) Reynolds dependence of third-order structure functions. Phys Fluids 16(2):482–485

George WK (1992) The decay of homogeneous isotropic turbulence. Phys Fluids 4:1492–1509

George WK, Wang H, Wollbald C, Johansson TG (2001) Homogeneous turbulence and its relation to realizable flows. In: Proceedings of the 14th Australasian fluid mechanics conference, Adelaide University, pp. 41–48

von Kármán T and Howarth L (1938) On the statistical theory of isotropic turbulence. Proc R Soc London Ser A 164:192–215

Kim J, Antonia RA (1993) Isotropy of the small scales of turbulence at low Reynolds number. J Fluid Mech 251:219–238

Lavoie P, Burattini P, Djenidi L, Antonia RA (2005) Effect of initial conditions on decaying grid turbulence at low R_λ. Exp Fluids 39:865–874

Lavoie P, Djenidi L, Antonia RA (2007) Effects of initial conditions in decaying turbulence generated by passive grids. J Fluid Mech (Accepted for publication)

Laws EM, Livesey JL (1978) Flow through screens. Annu Rev Fluid Mech 10:247–266

Moin P, Mahesh K (1998) Direct numerical simulation: a tool in turbulence research. Annu Rev Fluid Mech 30:539–578

Müller E, Nobach H, Tropea C (1998) Model parameter estimation from non-equidistant sampled data sets at low data rates. Meas Sci Technol 9:435–441

Mydlarski L, Warhaft Z (1996) On the onset of high-Reynolds-number grid-generated wind tunnel turbulence. J Fluid Mech 320:331–368

Nogueira J, Lecuona A, Rodriguez PA (1999) Local field correction PIV: on the increase of accuracy of digital PIV systems. Exp Fluids 27:107–116

Poelma C, Westerweel J, Ooms G (2006) Turbulence statistics from optical whole-field measurements in particle-laden turbulence. Exp Fluids 40: 347–363

Romano GP, Antonia RA, Zhou T (1999) Evaluation of LDA temporal and spatial velocity structure functions in a low Reynolds number turbulent channel flow. Exp Fluids 27:368–377

Saarenrinne P, Piirto M (2000) Turbulent kinetic energy dissipation rate estimation from PIV velocity vector fields. Exp Fluids (Suppl) S300–S307

Saffman PG (1968) Lectures on homogeneous turbulence. In: Zabusky N (ed) Topics in nonlinear physics. Springer, Heidelberg, pp 485–614

Saikrishnan N, Marusic I, Longmire EK (2006) Assessment of dual plane PIV measurements in wall turbulence using DNS data. Exp Fluids 41:265–278

Scarano F (2003) Theory of non-isotropic spatial resolution in PIV. Exp Fluids 35:268–277

Sirivat A, Warhaft Z (1983) The effect of a passive cross-stream temperature gradient on the evolution of temperature variance and heat flux in grid turbulence. J Fluid Mech 128:323–346

Suzuki Y, Kasagi N (1992) Evaluation of hot-wire measurements in wall shear turbulence using a direct numerical simulation database. Exp Therm Fluid Sci 5:69–77

Tennekes H, Lumley JL (1972) A first course in turbulence. MIT Press, Cambridge

Van Maanen HRE, Nobach H, Benedict LH (1999) Improved estimator for the slotted autocorrelation function of randomly sampled LDA data. Meas Sci Technol 10:L4–L7

Westerweel J, Dabiri D, Gharib M (1997) The effect of a discrete window offset on the accuracy of cross-correlation analysis of digital PIV recordings. Exp Fluids 23:20–28

Wyngaard JC (1968) Measurement of small-scale turbulence structures with hot wires. J Sci Instrum 1:1105–1108

Zhou T, Antonia RA (2000a) Reynolds number dependence of the small-scale structure of grid turbulence. J Fluid Mech 406:81–107

Zhou T, Antonia RA (2000b) Approximations for turbulent energy and temperature variance dissipation rates in grid turbulence. Phys Fluids 12(2):335–344

Zhou T, Antonia RA, Lasserre J-J, Coantic M, Anselmet F (2003) Transverse velocity and temperature derivative measurements in grid turbulence. Exp Fluids 34:449–459

Zhu Y, Antonia RA (1995) Effect of wire separation on X-probe measurements in a turbulent flow. J Fluid Mech 287: 199–223

Zhu Y, Antonia RA (1996) The spatial resolution of hot-wire arrays for the measurement of small-scale turbulence. Meas Sci Technol 7:1349–1359